The study on the transport efficiency of effective excitons and relationship with the thickness of active materials

XI XI[a,b,c] , XIAOJING CHEN[b], GUILIUN LIU[a,c], YING GUO[a,c], GUOHUA LI[a,c,*]
[a]*School of Science, Jiangnan University, 1800 Lihu Ave., Wuxi, China, 214122*
[b]*Suntech Power Co., Ltd., 12 Xinhua Road, Wuxi, China, 214028*
[c]*Jiangsu (Suntech) Institute for Photovoltaic Technology, 12 Xinhua Road, Wuxi, China, 214028*

Organic solar cells are attracting a great deal of attention now. However, the academic system of organic solar cells is still not so perfect. Most analysis of exciton recombination was still on the qualitative process. In this paper, a concept of effective exciton transport efficiency was given, based on the generation rate of effective excitons. Using this method, the error between the simulation of effective exciton generation rate and practical experiments was explained more clearly. With the increase of the active layers' thicknesses, the electrode interface would leave farther away from the effective exciton generation region. This made less influence of electrode interface to the effective excitons, and the transport efficiency increased. Although this decreased the effective exciton generation rate a little, the performances of cells still can get better. The transport efficiency also can explain the function of electrode buffer layers, as well as the superiority of C_{70} acceptor to that of C_{60}.

1. Introduction

Organic solar cells (OSCs) are attracting a great deal of attention, because of flexibility, low cost, light weight, and large area application [1-11]. From the first double-layer structured solar cell introduced by Tang [12], different methods have been proposed in order to improve the power conversion efficiency and the stability of organic solar cells. The mechanism can be roughly concluded into three processes [13]: 1) the generation of excitons; 2) exciton dissociation; 3) carrier collection. Many efforts have been made to increase the efficiency. However, the academic system of organic solar cells is not so perfect now. Reference [14] gave the concept of effective exciton generation rate. Maximizing this rate, the best thickness combination was obtained. But a small error of this method still exists to the practical experiments. The error was brought from the recombination of excitons. In Reference [14], the error analysis was simply given. In this paper, a concept of the transport efficiency of effective excitons was given. The error between the simulation and experiments in Reference [14] was analyzed in detail based on this concept. The influence of the electrode interfaces to the excitons was represented by the transport efficiency.

2. Modeling

The concept of effective exciton is from Reference [14]. The excitons which can diffuse to the donor/acceptor (D/A) interface and be dissociated into free carriers are called effective excitons. From this concept, the effective exciton generation area is in the range which is no more than one exciton diffusion length away from the D/A interface inside the donor and acceptor layers respectively.

The number of absorption photons at a unit area per second is

$$P = \frac{\pi \varepsilon_0 \kappa n}{h} \left| \tilde{E} \right|^2 \tag{1}$$

where ε_0 and c are the dielectric constant and light speed in vacuum, respectively. $\left| \tilde{E} \right|^2$ is the light intensity distribution. n and κ are the refractive index and the extinction coefficient. Assuming that all these photons can be used to produce excitons, then the exciton generation rate at the position x at a unit area, inside the material j, after absorbing the light with the wavelength of λ is,

$$g_{\lambda,j}(x) = \frac{\pi \varepsilon_0}{h} \kappa_{\lambda,j} n_{\lambda,j} \left| \tilde{E}_{\lambda,j}(x) \right|^2 \tag{2}$$

The actual sunlight energy, as well as the photon flux density, is not a uniform distribution over wavelengths. Additionally, the substrate, usually glass is used, does not

show a uniform transmissivity either. So far, an actual effect of $g_{\lambda,j}(x)$ needs to be improved to

$$g_{\lambda,j}(x) = \frac{\pi\varepsilon_0}{h}\Phi_\lambda T_\lambda \kappa_{\lambda,j} n_{\lambda,j}\left|\tilde{E}_{\lambda,j}(x)\right|^2 \qquad (3)$$

where Φ_λ is the photon flux density of AM1.5G at wavelength λ, and T_λ is the transmissivity of substrates at this wavelength.

Thus, for the space range which is within an exciton diffusion length inside donor and acceptor layers near the D/A interface and the response wavelength of the device range ($[\lambda_1, \lambda_2]$) of the device, the total exciton generation rate can be described as

$$G = \int_{x_{D/A}-\min[d_D,L_D]}^{x_{D/A}+\min[d_A,L_A]}\left[\int_{\lambda_1}^{\lambda_2} C\Phi_\lambda T_\lambda \kappa_{\lambda,j} n_{\lambda,j}\left|\tilde{E}_{\lambda,j}(x)\right|^2 d\lambda\right]dx \qquad (4)$$

where $x_{D/A}$ is the position of the D/A interface; d_A, d_D are the thicknesses of acceptor and donor, respectively. The response of the device is from the light wavelength of λ_1 to λ_2. L_D and L_A are the exciton diffusion lengths of donor and acceptor respectively.

Here, the photon flux distribution and transmittivity of the substrate have been considered. And it is much closer to the actual application.

Only the generation of excitons has been considered in Eq. (4). The recombination has not been exhibited. So in Reference [14], there was a small error between the calculation results and practical experiments. The recombination of effective excitons can be evaluated by its transport efficiency.

In Eq. (4), the light intensity $\left|\tilde{E}_{\lambda,j}(x)\right|^2$ here is a relative value. And sometimes some parameters, such as Φ_λ also can use relative data. So assuming a parameter (S_t), which the absolute value of effective exciton generation rate (V_{EEG}) can be written as $V_{EEG} = G \cdot S_t$. If all the effective excitons can be separated into free carriers, and all the carriers can be collected easily, the current density of the device will be maximum,

$$J_{ph}^{Max} = 2V_{EEG}\cdot q = 2q\cdot S_t\cdot G \qquad (5)$$

where q is the electron charge, "2" means a positive charge (hole) and a negative charge (electron) appear by the dissociation of an exciton.

The device current is mostly determined by the generation of effective excitons and their transport efficiency. Here assuming the carrier transport efficiency and collection efficiency are 100% [13].

J_{sc}, the short circuit current density of the device, is the maximum working current. Thus the transport efficiency of effective excitons can be concluded as,

$$\eta_{Tran} = \frac{J_{sc}}{J_{ph}^{Max}} = \frac{J_{sc}}{2q\cdot G\cdot S_t} \qquad (6)$$

3. Experiments, results and discussion

The cells were fabricated in a typical sandwich structure. The ITO-Glass were sequentially cleaned by ultrasonic treatment in acetone, isopropyl alcohol and deionized water, and blown by N_2 gas, and treated by UN-Ozone for 15 min. The UV wavelength used here was 185 nm. The power of the UV lamp was 20 W, which was put in an airtight box with the capacity of about 40 L. Ozone gas was generated by using UV light to excite oxygen in air inside the box. The temperature and humidity inside the box were always kept at 20 ℃ and 30%, respectively.

The purities of CuPc, C_{60} and C_{70} were 98.5%, 99.9%+ and 99.9%+, respectively. And they were not further purified before experiments. All the layers in OSCs were fabricated by vacuum evaporation at a pressure of 2.5×10^{-3} Pa. The thicknesses of the layers were monitored by a quartz oscillator thickness monitor and they were also checked by an ellipsometer. PEDOT:PSS solution (1.3 wt% dispersed in H_2O, conductive grade) was spin-coated on the ITO electrode at 5000 rpm for 30 s, and annealed at 120 ℃ for 15 min. The average thickness of this layer was 40.2 nm measured by an ellipsometer.

The active area of the device was about 0.06 cm^2. The current-voltage characteristics were measured with a Keithley 2400 sourcemeter, under an illumination of 100 mW/cm^2 (monitored by a standard polysilicon solar cell) with an AM1.5G sun simulator.

A very accurate thickness control in the experiments was too difficult here. So the thickness of 5 nm for active materials was used as a thickness step. The uniformity for an ultrathin film is a big problem. Thus, the thicknesses of active materials started from 15 nm.

The performances of the cells were not good. This was due to the limitation of equipments. It had to break the vacuum and open the equipment cavity to change the evaporation material after finishing depositing a layer. Too much pollution was introduced in the fabrication process, so the power conversion efficiencies were several times lower than those reported. However, relative results still can clearly describe the issues.

The transmittivity spectrum of the glass substrate and the photon flux density of AM1.5G were used in the simulation. They were shown in Fig. 1, where Φ_λ was a relative value. The photon flux density at each wavelength in Fig. 1 was related to the one at 550 nm. The data was 4.3243×10^{14} ((cm^{2}s)$^{-1}$).
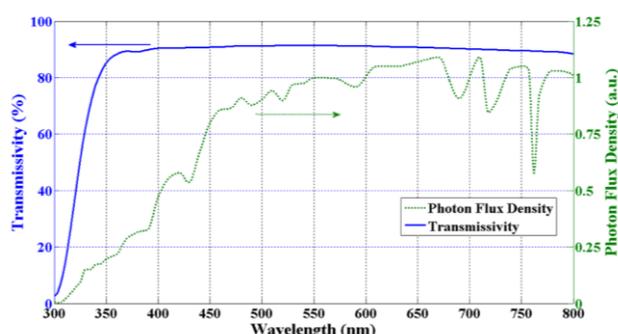
Fig. 1. The transmissivity spectrum of the glass substrate and the photon flux density of AM1.5G The photon flux density at each wavelength is related to the one at 550 nm. The data is 4.3243×10^{14} ((cm^{2}s)$^{-1}$) from "IEC 60904–3: 2008, ASTM G-173-03 global".

First, take the ITO/CuPc/C$_{60}$/Al cell as an example.

From the method in Reference [14], the best thickness combination of donor and acceptor was CuPc(16 nm)/C$_{60}$(32 nm). The practical results were shown in Table 1.

Table 1. Comparison of characteristics of cells with different CuPc and C$_{60}$ thicknesses.

Structure	J_{sc} mA/cm^2	V_{oc} mV	FF	η %
CuPc(10 nm)/C$_{60}$(30 nm)	1.22	461	0.288	0.1620
CuPc(15 nm)/C$_{60}$(30 nm)	1.28	455	0.294	0.1712
CuPc(20 nm)/C$_{60}$(30 nm)	1.36	462	0.295	0.1854
CuPc(25 nm)/C$_{60}$(30 nm)	1.27	461	0.291	0.1704
CuPc(10 nm)/C$_{60}$(35 nm)	1.24	460	0.290	0.1654
CuPc(15 nm)/C$_{60}$(35 nm)	1.32	461	0.294	0.1789
CuPc(20 nm)/C$_{60}$(35 nm)	1.38	470	0.295	0.1913
CuPc(25 nm)/C$_{60}$(35 nm)	1.34	460	0.287	0.1769
CuPc(10 nm)/C$_{60}$(40 nm)	1.29	456	0.292	0.1718
CuPc(15 nm)/C$_{60}$(40 nm)	1.34	466	0.293	0.1830
CuPc(20 nm)/C$_{60}$(40 nm)	1.41	472	0.297	0.1977
CuPc(25 nm)/C$_{60}$(40 nm)	1.35	462	0.286	0.1784
CuPc(10 nm)/C$_{60}$(45 nm)	1.23	455	0.292	0.1634
CuPc(15 nm)/C$_{60}$(45 nm)	1.28	459	0.285	0.1674
CuPc(20 nm)/C$_{60}$(45 nm)	1.32	466	0.276	0.1698
CuPc(25 nm)/C$_{60}$(45 nm)	1.27	455	0.275	0.1589

The best actual result was CuPc(20 nm)/C$_{60}$(40 nm), a little thicker than the calculation result. And this rule also agreed with Reference [14].

The structure of CuPc(15 nm)/C$_{60}$(30 nm) was the closest to the theoretic data. Here, $G=2.55\times10^{26}$ (a.u.) and $\eta_{Tran}=1.57\times10^{-7}/S_t$. "$G$" for the best actual cell was 2.28×10^{26} (a.u.), while "η_{Tran}" for this cell was $1.93\times10^{-7}/S_t$. So the transport efficiency of effective excitons increased when the active layers grew thicker, though the generation rate of effective excitons would decrease. The thicker cell in Table 1 [CuPc(25 nm)/C$_{60}$(45 nm)], "η_{Tran}" was $2.06\times10^{-7}/S_t$ for this cell, even much higher. But "G" here

was only 2.28×10^{26} (a.u.). So the lower "G" made this cell perform not very well, although "η_{Tran}" was the highest here.

The relationship between "η_{Tran}" and the active layers' thicknesses was concluded as, thicker layers, higher "η_{Tran}".

At the interface of C$_{60}$/Al, inside the C$_{60}$ layer, Al atoms may infiltrate into the active layer, even "C-Al" bonds were formed [15]. Lots of excitons were recombined here. This area may not be the effective exciton generation region. But the density of exciton here was lower, since a high recombination rate. Then, a

density gradient was formed. In the effective exciton generation region, a higher exciton density existed. Many effective excitons would diffuse to the C_{60}/Al interface and be recombined (see Fig. 2). It made the loss of effective excitons. And this loss was not been exhibited in Eq. (4).
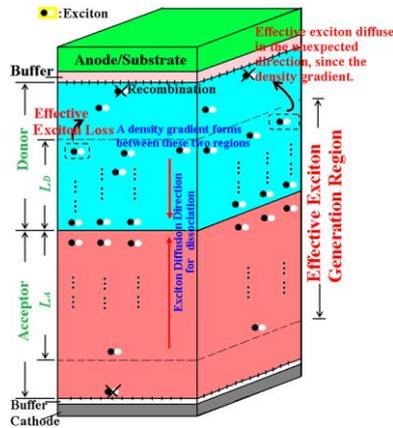
Fig. 2. Sketch map of the loss of effective excitons

If the thickness grew a little thicker, the interface of C_{60}/Al would leave farther away from the effective exciton generation region and make less influence to the effective excitons. This made "η_{Tran}" increase.

The same reason for the thickness of CuPc also existed, only the carriers were changed from electrons into holes.

Electron buffer layer can evidently decrease the exciton recombination rate at the interface. So next, the effective exciton transport efficiency for the cell with cathode buffer layer was investigated. An ITO/CuPc/C_{60}/LiF/Al cell was taken as an example. The LiF thickness was 1.5 nm.

From the method in Reference [14], the best thickness combination of the active layers was CuPc(16 nm)/C_{60}(32 nm). The thickness of CuPc and C_{60} were the same with the cell without cathode buffer layer. So this ultrathin buffer did not change the light intensity distribution inside the cells. For the best calculated structure, "G" was 2.588×10^{26} (a.u.). Since the cell had no anode buffers, the thickness of CuPc in practical was fixed at 20 nm as above, shifting the thickness of C_{60} from 30 nm to 40 nm. Table 2 gave the performances of the cells as well as "G" and "η_{Tran}".

Table 2. The characteristics of the cells with different active layer thickness, in which a 1.5 nm thick LiF cathode buffer layer is inserted (AM1.5G, 100 mW/cm^2)

Structure	J_{sc} mA/cm^2	V_{oc} mV	FF	η %	G a.u.	η_{Tran}
CuPc(20 nm)/C_{60}(30 nm)/LiF	1.72	512	0.324	0.2853	2.44×10^{26}	$2.20 \times 10^{-7}/S_t$
CuPc(20 nm)/C_{60}(35 nm) /LiF	1.81	516	0.326	0.3045	2.42×10^{26}	$2.34 \times 10^{-7}/S_t$
CuPc(20 nm)/C_{60}(40 nm) /LiF	1.76	518	0.323	0.2945	2.25×10^{26}	$2.44 \times 10^{-7}/S_t$

The results in Table 2 were the same with that of the cell without LiF cathode buffer layer, a thicker acceptor layer, a lower effective exciton recombination it was. Or it can be said that a high transport efficiency of effective excitons was exhibited.

The function of LiF cathode buffer layer also can be reflected by the effective exciton transport efficiency. For the same active layers' thicknesses, "η_{Tran}" of CuPc(20 nm)/C_{60}(40 nm) /LiF was a little higher than that of CuPc(20 nm)/C_{60}(40 nm) ($2.44 \times 10^{-7}/S_t > 1.93 \times 10^{-7}/S_t$).

Increasing the layer thickness did improve the effective exciton transport efficiency, but it would decrease the generation rate of effective excitons. Since the improvement at C_{60}/Al interface by LiF layer, the loss of excitons was evidentially reduced. So a large distance between the electrode and effective exciton generation region was not needed. From Table 2, it was seen that the acceptor layer's thickness can be reduced to 35 nm, when LiF layer is introduced. "η_{Tran}" of this cell (CuPc(20 nm)/C_{60}(35 nm) /LiF) was still higher than that of the best actual cell without LiF buffer (CuPc(20 nm)/C_{60}(40 nm) $1.93 \times 10^{-7}/S_t$). Thus, "η_{Tran}" was still increased by using electrode buffers, even though the active layers' thicknesses reduce a little.

The transport efficiency of effective excitons would go on increasing, when an anode buffer (PEDOT:PSS — 40 nm) was used. From the method in Reference [14], the best thickness was ITO/PEDOT:PSS/CuPc(16 nm)/C_{60}(26 nm)/LiF(1.5 nm)/Al. "G" for this cell is 2.417×10^{26} (a.u.). Table 3 gave the performances of the cells.

Table 3. The characteristics of the cells with different active layer thickness which insert a PEDOT:PSS anode buffer layer (AM1.5G, 100 mW/cm^2)

Structure	J_{sc} mA/cm^2	V_{oc} mV	FF	η %	G a.u.	η_{Tran}
PEDOT:PSS/CuPc(15 nm)/C$_{60}$(25 nm)/LiF	3.08	516	0.362	0.5753	2.409×10^{26}	3.99×10^{-7}/S_t
PEDOT:PSS/CuPc(20 nm)/C$_{60}$(30 nm)/LiF	3.24	516	0.360	0.6019	2.396×10^{26}	4.23×10^{-7}/S_t
PEDOT:PSS/CuPc(20 nm)/C$_{60}$(35 nm)/LiF	3.20	525	0.352	0.5914	2.364×10^{26}	4.32×10^{-7}/S_t

A large improvement of "η_{Tran}" was seen by using PEDOT:PSS buffer. And the reasons were similar as LiF cathode buffer. Here, the recombination of excitons was reduced a lot at the anode interface.

From the analysis above, thickness of CuPc should be reduced, just like the thickness of C$_{60}$ when LiF buffer was introduced. However, since the thickness of CuPc was too thin, the reduction was limited. The thickness step of 5 nm in the experiments can not reflect this tiny reduction.

The thickness of PEDOT:PSS was much higher than that of LiF cathode buffer. So the light intensity distribution was surely changed. Synthetically considering "G" and "η_{Tran}", the thickness of C$_{60}$ was only 30 nm in practical.

In Reference [16], the performances of small molecule organic solar cells based on CuPc/C$_{60}$ and CuPc/C$_{70}$ was studied. C$_{70}$ was superior to C$_{60}$. The performances of CuPc/C$_{70}$ cells were shown in Table 4. For an ITO/PEDOT:PSS(40 nm)/LiF(1 nm)/CuPc/C$_{70}$/LiF(1.5 nm)/Al cell, the maximum generation rate of effective excitons ("G") was 2.792×10^{26} (a.u.), appeared at CuPc(16 nm)/C$_{70}$(19 nm).

Table 4. The J–V characteristics of the devices with different C$_{70}$ thickness (AM1.5G, 100 mW/cm^2)

Structure	J_{sc} mA/cm^2	V_{oc} mV	FF	η %	G a.u.	η_{Tran}
PEDOT:PSS/LiF/CuPc(20 nm)/C$_{70}$(20 nm)/LiF	3.72	602	0.412	0.9226	2.785×10^{26}	4.17×10^{-7}/S_t
PEDOT:PSS/LiF/CuPc(20 nm)/C$_{70}$(25 nm)/LiF	3.81	608	0.415	0.9613	2.768×10^{26}	4.30×10^{-7}/S_t
PEDOT:PSS/LiF/CuPc(20 nm)/C$_{70}$(30 nm)/LiF	3.74	612	0.408	0.9339	2.709×10^{26}	4.32×10^{-7}/S_t

The same rule of "η_{Tran}" was been shown.

From Table 4 the generation rate of effective excitons ("G") of CuPc/C$_{70}$ cell was larger than that of CuPc/C$_{60}$ cell. Larger "G" was good for the design of devices. And this agreed with Reference [16]. Using C$_{70}$ as an acceptor can increase the photovoltaic characteristics. Meanwhile, the "η_{Tran}" of CuPc/C$_{70}$ cell was a little higher than that of the CuPc/C$_{60}$ cell (Table 3), even at a thinner acceptor layer thickness condition. This also can reflect the superiority of C$_{70}$.

4. Conclusion

A concept of effective exciton transport efficiency was given in this paper. This efficiency was related to the generation and recombination of effective excitons. Reference [14] gave the concept of effective exciton generation rate. In the simulation design, when the highest generation rate was reached, the best performances and thickness combination were obtained. However, there was a small error between the simulation and experiments. Using the method of effective exciton transport efficiency, this error was explained more clearly.

Increasing the thickness of active layer, the transport efficiency of effective excitons would be improved. Although this would decrease the effective exciton generation rate, the performances of cells were still better. Excitons were recombined seriously at the electrode interfaces. Then an exciton density gradient was formed. Therefore, many effective excitons would diffuse from the effective exciton generation region to the electrode interfaces and it made the loss of effective excitons. If the thickness grew a little thicker, the electrode interface would leave farther away from the effective exciton generation region. This would make less influence to the effective excitons, and the effective exciton transport efficiency would increase.

The transport efficiency also can explain the function of electrode buffer layers. The transport efficiency increased a lot when the buffer was introduced, because of a lower recombination rate of excitons near the electrode interface. Meanwhile, since a higher effective exciton transport efficiency was obtained after introducing electrode buffers, the active layers' thicknesses were closer to the simulation results, and a higher effective exciton generation rate were obtained.

Additionally, the superiority of C_{70} than C_{60} was also explained by effective exciton transport efficiency and effective exciton generation rate, and agreed with Reference [16].

References

[1] G. Yu, J. Gao, J.C. Hummelen, F. Wudl, A. J. Heeger, Science **270**, 1789 (1995).

[2] C. J. Brabec, Sol. Energy Mater. Sol. Cells **83**, 273 (2004).

[3] C. Lungenschmied, G. Dennler, H. Neugebauer, S. N. Sariciftci, M. Glatthaar, T. Meyer, A. Meyer, Sol. Energy Mater. Sol. Cells **91**, 379 (2007).

[4] M. Niggemann, B. Zimmermann, J. Haschke, M. Glatthaar, A. Gombert, Thin Solid Films **516**, 7181 (2008).

[5] F. C. Krebs, H. Spanggard, T. Kjaer, M. Biancardo, J. Alstrup, Mater. Sci. Eng. B **138**, 106 (2007).

[6] M. Jørgensen, O. Hagemann, J. Alstrup, F. C. Krebs, Sol. Energy Mater. Sol. Cells **93**, 413 (2009).

[7] F. C. Krebs, Sol. Energy Mater. Sol. Cells **93**, 465 (2009).

[8] F. C. Krebs, M. Jørgensen, K. Norrman, O. Hagemann, J. Alstrup, T. D. Nielsen, J. Fyenbo, K. Larsen, J. Kristensen, Sol. Energy Mater. Sol. Cells **93**, 422 (2009).

[9] L. Blankenburg, K. Schultheis, H. Schache, S. Sensfuss, M. Schöodner, Sol. Energy Mater. Sol. Cells **93**, 476 (2009).

[10] F. C. Krebs, J. Fyenbo, M. Jorgensen, Journal Material Chemistry. **20**, 8994 (2010).

[11] N. C. Miller, S. Sweetnam, E. T. Hoke, R. Gysel, C. E. Miller, J. A. Bartelt, X. Xie, M. F. Toney, M. D. McGehee, Nano Letters, **12**, 1566 (2012).

[12] C. W. Tang, Appl. Phys. Lett. **48**, 183 (1986).

[13] P. Peumans, A. Yakimov, S. R. Forrest, Journal of applied physics, **93**, 3693 (2003).

[14] Xi Xi, Jiaqi Wu, Wenjia Li, Jingjia Ji, Zhengrong Shi, Guohua Li, 2010 10th IEEE International Conference on Solid-State and Integrated Circuit Technology, 1286-1288.

[15] M. Jørgense, K. Norrman, F. C. Krebs, Solar Energy Materials & Solar Cells, **92**, 686 (2008).

[16] X. Xi, W. J. Li, J. Q. Wu, J. J. Ji, Z. R. Shi, G. H. Li, Solar Energy Materials and Solar Cells, **94**, 2435 (2010).

---

[*]Corresponding author: xi_xi_hunt@aliyun.com